

Cycloaddition Reactions

On the Critical Effect of the Metal (Mo vs. W) on the [3+2] Cycloaddition Reaction of M_3S_4 Clusters with Alkynes: Insights from Experiment and TheoryEmilio Bustelo,^[a] Artem L. Gushchin,^[b] M. Jesús Fernández-Trujillo,^[a] Manuel G. Basallote,^{*[a]} and Andrés G. Algarra^{*[c]}

Abstract: Whereas the cluster $[Mo_3S_4(acac)_3(py)_3]^+$ ($[1]^+$, acac = acetylacetonate, py = pyridine) reacts with a variety of alkynes, the cluster $[W_3S_4(acac)_3(py)_3]^+$ ($[2]^+$) remains unaffected under the same conditions. The reactions of cluster $[1]^+$ show polyphasic kinetics, and in all cases clusters bearing a bridging dithiolene moiety are formed in the first step through the concerted [3+2] cycloaddition between the $C\equiv C$ atoms of the alkyne and a $Mo(\mu-S)_2$ moiety of the cluster. A computational study has been conducted to analyze the effect of the metal on these concerted [3+2] cycloaddition reactions. The calculations suggest that the reactions of cluster $[2]^+$ with alkynes feature ΔG^\ddagger values only slightly larger than its molybdenum analogue, however, the differences in the reaction free energies between both metal clus-

ters and the same alkyne reach up to approximately 10 kcal mol⁻¹, therefore indicating that the differences in the reactivity are essentially thermodynamic. The activation strain model (ASM) has been used to get more insights into the critical effect of the metal center in these cycloadditions, and the results reveal that the change in reactivity is entirely explained on the basis of the differences in the interaction energies E_{int} between the cluster and the alkyne. Further decomposition of the E_{int} values through the localized molecular orbital-energy decomposition analysis (LMO-EDA) indicates that substitution of the Mo atoms in cluster $[1]^+$ by W induces changes in the electronic structure of the cluster that result in weaker intra- and inter-fragment orbital interactions.

Introduction

The formation and activation of C–S bonds has been thoroughly studied for decades due to its importance in chemistry. Organosulfur compounds are widely present in natural products and pharmaceutical compounds, and therefore the development of cost-efficient and improved ways to introduce sulfur atoms onto target molecules represents a long sought-after goal in biomimetic and pharmaceutical chemistry.^[1] In contrast, the removal of sulfur from fossil fuels is one of the most important steps in the modern refinement of petroleum. For both technical and environmental reasons, more and more

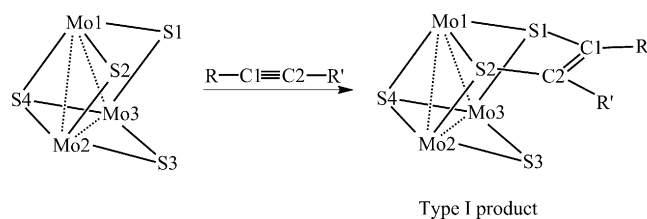
stringent regulations have been introduced in many countries to reduce the sulfur content in fuels, and as a result more efficient hydrodesulfurisation catalysts are currently required.^[2] Notably, an increasing proportion of the documented studies involve the use of transition-metal (TM) complexes, as they generally provide a more efficient way to carry out these transformations.^[1h,3] Especially fascinating are the achievements made in the construction of C–S bonds, where several catalytic systems have been successfully developed and applied in organic synthesis.^[4] However, the mechanistic understanding of TM-mediated C–S bond formation and breaking is far less comprehensive in comparison to analogous C–C or C–N processes, and more research is clearly required. In the last few years we have been interested in the reactivity of M_3S_4 ($M = Mo, W$) cuboidal clusters with alkynes, which leads to species with new C–S bonds. The reaction was initially reported by Shibahara et al. in the 1990s, when it was proposed that type I reaction products (Scheme 1) are formed initially in a concerted process, whereas for some tungsten complexes subsequent protonation and addition of a second alkyne can generate additional products.^[5] By means of combined experimental and computational studies, we have recently confirmed the proposal of Shibahara and concluded that the formation of type I products can be described as a concerted [3+2] cycloaddition reaction between a $M(\mu-S)_2$ moiety of the cluster and the $C\equiv C$ bond of the alkyne (Scheme 1), that is, both C–S bonds are

[a] Dr. E. Bustelo, Dr. M. J. Fernández-Trujillo, Prof. Dr. M. G. Basallote
Departamento de Ciencia de los Materiales
e Ingeniería Metalúrgica y Química Inorgánica
Campus Universitario de Puerto Real, Universidad de Cádiz
11510 Puerto Real, Cádiz (Spain)
E-mail: manuel.basallote@uca.es

[b] Dr. A. L. Gushchin
Nikolae Institute of Inorganic Chemistry, Russian Academy of Sciences
Novosibirsk State University, 630090 Novosibirsk (Russia)

[c] Dr. A. G. Algarra
Department of Organic Chemistry, Arrhenius Laboratory
Stockholm University, 10691 Stockholm (Sweden)
E-mail: andres.algarra@uca.es

Supporting information for this article is available on the WWW under <http://dx.doi.org/10.1002/chem.201502644>.



Scheme 1. Reaction between a Mo_3S_4 cluster and an alkyne.

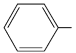
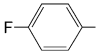
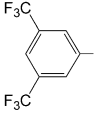
formed in a single step and no intermediates with one C–S bond can be characterized.^[6,7]

Knowledge of the kinetic–mechanistic properties of these reactions is not only interesting in relation to the alkyne activation and C–S bond formation, but also because these reactions could be used as novel click reactions for the incorporation of cuboidal clusters into more complex structures, with new reactivities and catalytic properties. In fact, Shibahara et al. have also shown recently that the addition of dmad (see Table 1 for a list of the investigated alkynes and their abbreviations) to Mo_3S_4 clusters leads to type I products able to α,α -dehydrogenate solvent molecules such as acetone, acetaldehyde, ethyl acetoacetate, and acetophenone.^[5g] In addition, metal–dithiolene links represent the basic structural motif of a number of Mo and W enzymes able to catalyze a variety of processes in biological substrates, including oxygen-atom transfer reactions,^[8] and Llusar et al. have shown that clusters containing coordinated dithiolenes also present interesting electronic properties.^[9] From a computational point of view these systems are also highly attractive due to the possibility of analyzing the effect of the metal moiety on the concerted double C–S bond formation that leads to MS_2C_2 five-membered rings.^[10] The experiments in acetonitrile solutions carried out in previous work have already revealed the dramatic effect of the R group of the alkyne [$\text{R}-\text{C}\equiv\text{C}-\text{R}$; $\text{R}=\text{CH}_2\text{OH}$ (btd); COOH (adc)] on the kinetics of the reaction with $[\text{Mo}_3\text{S}_4(\text{acac})_3(\text{py})_3]^+$ ($[1]^+$) (acac = acetylacetonate, py = pyridine), which showed a rate constant three orders of magnitude faster with adc than with btd.^[7] This was thoroughly analyzed by combining an activation strain model (ASM)^[11] analysis with frontier molecular orbital (FMO) calculations, and the results indicated that the major difference in the activation barrier for the reaction with both alkynes originates from their different degree of interaction with the cluster at the transition-state geometries. In the framework of the frontier molecular orbital theory the effect was traced to the differences in the frontier orbitals of the alkynes, which in the case of adc become closer to those of the cluster and allow for a stronger orbital interaction.

To gain further insight into the mechanism of these processes, here we decided to extend the work in two directions. First, the metal center in the cluster $[1]^+$ was changed to tungsten, but the resulting cluster $[\text{W}_3\text{S}_4(\text{acac})_3(\text{py})_3]^+$ ($[2]^+$) was found to be unable to react with the previously tested alkynes adc and btd. Subsequent attempts with other internal and terminal al-

kynes, the names and abbreviations of them are given in Table 1, were also unsuccessful, whereas the Mo cluster $[1]^+$ reacted with all of them. The kinetics of the latter reactions have been monitored and the reaction product of cluster $[1]^+$ with dmad has been isolated and characterized as a type I adduct. Thus, the results obtained in the present work reveal that the nature of the metal center plays a critical role in the [3+2] cycloaddition process despite not being directly involved in any bond formation or undergoing changes in its coordination

Table 1. List of the alkynes employed in this work.

Full name	Abbreviation	R–C \equiv C–R'	
		R	R'
propargyl alcohol	PrA	–H	–CH ₂ OH
2-butyne-1,4-diol	btd	–CH ₂ OH	–CH ₂ OH
acetylene dicarboxylic acid	adc	–COOH	–COOH
dimethyl acetylenedicarboxylate	dmad	–COOCH ₃	–COOCH ₃
phenylacetylene	PhA		–H
1-ethynyl-4-fluorobenzene	^F PhA		–H
1-ethynyl-3,5-bis(trifluoromethyl) benzene	^{CF₃} PhA		–H

kyne sphere. This represents an excellent system to computationally analyze the effect of the metal center on the reaction, and a thorough DFT study aimed at understanding the reasons of this behavior has also been carried out.

Results and Discussion

The reaction of clusters $[1]^+$ and $[2]^+$ with alkynes

Kinetic studies

The molybdenum and tungsten incomplete cubane clusters $[1]\text{PF}_6$ and $[2]\text{PF}_6$ have been tested against a variety of internal and terminal alkynes. The reaction of $[1]\text{PF}_6$ with adc and btd has been reported previously,^[7] and we were interested in checking the reactivity of the analogous tungsten cluster $[2]\text{PF}_6$. Notably, $[2]^+$ does not react in acetonitrile solution, neither with adc or btd, nor with any of the other alkynes included in Table 1. In contrast, cluster $[1]^+$ does react with all the new alkynes tested, both symmetrical (i.e., dmad) and asymmetrical (i.e., PrA, PhA, ^FPhA, and ^{CF₃}PhA). This is in line with previous results showing that the aqua cluster $[\text{Mo}_3\text{S}_4(\text{H}_2\text{O})_9]^{4+}$ reacts with acetylene leading to the corresponding type I product,^[5b] whereas the tungsten analogue does not.^[5c]

Thus, the reaction of cluster $[1]^+$ with an excess of dmad occurs initially with spectral changes as those illustrated in Figure 1. Stopped-flow experiments show the appearance of a band at $\lambda=870$ nm, which disappears in a much slower process that must be monitored with a conventional spectrophotometer. The stopped-flow data can be satisfactorily fitted to

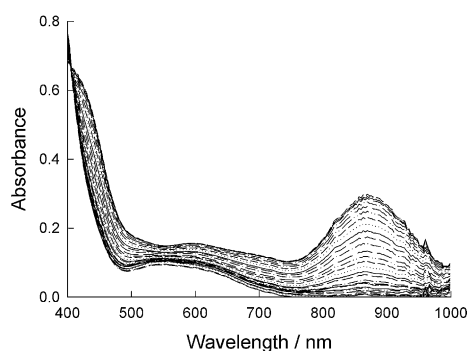


Figure 1. Typical spectral changes in the stopped-flow time scale for the reaction of cluster $[1]^+$ with dmad in acetonitrile ($T = 25.0^\circ\text{C}$, $[1]^+ = 1.5 \times 10^{-4}\text{ M}$, $[\text{dmad}] = 0.017\text{ M}$, time base = 10 s).

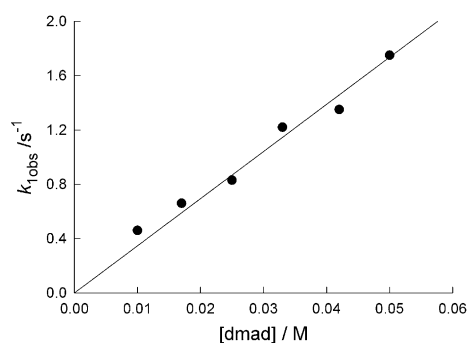


Figure 2. Plot of the dependence of the rate constant on the concentration of dmad for the first resolved kinetic step in the reaction of cluster $[1]^+$ with dmad in acetonitrile. The solid line corresponds to the fit of the data by using Equation (1).

a single kinetic step and the $k_{1\text{obs}}$ values show a linear dependence on the alkyne concentration [Figure 2, Eq. (1)] that leads to the second-order rate constant $k_1 = (35 \pm 1)\text{ M}^{-1}\text{ s}^{-1}$. The disappearance of the band at $\lambda = 870\text{ nm}$ also occurs in a single step, the values of $k_{2\text{obs}}$ showing saturation behavior with respect to the alkyne concentration (Figure 3). Fitting the data to Equation (2) leads to $k_2 = (3.4 \pm 0.4) \times 10^{-3}\text{ M}^{-1}\text{ s}^{-1}$ and $K = (38 \pm 5)\text{ M}^{-1}$.

The reaction with other alkynes (i.e., PrA, PhA, $^{\text{F}}\text{PhA}$, and $^{\text{CF}_3}\text{PhA}$) had to be monitored with a conventional spectrophotometer and also showed two kinetic steps that feature the appearance and subsequent disappearance of a band at $\lambda = 845\text{--}900\text{ nm}$ (Table 2). For some of the alkynes, the observed rate

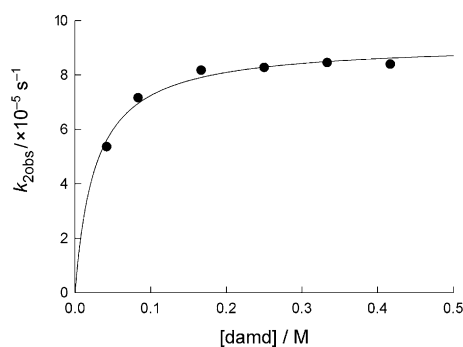


Figure 3. Plot of the dependence of the rate constants on the concentration of dmad for the second resolved kinetic step in the reaction of cluster $[1]^+$ with dmad in acetonitrile. The solid line corresponds to the fit of the data by using Equation (2).

constants for the first step can be satisfactorily fitted to Equation (1), whereas for PrA and PhA a non-zero intercept is clearly evident in the $k_{1\text{obs}}$ versus $[\text{alkyne}]$ plots (see the Supporting Information) and the data were fitted to Equation (3). The values of k_1 and k_{-1} for the different alkynes are included in Table 2.

With regard to the alkyne dependence of the $k_{2\text{obs}}$ values, saturation behavior is observed for dmad and PhA, whereas PrA and $^{\text{CF}_3}\text{PhA}$ show independence with respect to the alkyne. The data for the second step in the reaction of cluster $[1]^+$ with $^{\text{F}}\text{PhA}$ could not be satisfactorily fitted because the spectral changes for the disappearance of the cycloaddition product are masked by larger changes that probably correspond to a side reaction. It must be noted that for all the alkynes the

Table 2. Summary of the kinetic data for the reaction of cluster $[1]^+$ with different alkynes in acetonitrile or dichloromethane solutions at 25.0°C .

Alkyne	Solvent	λ [nm] ^[a]	k_1 [$\text{M}^{-1}\text{ s}^{-1}$] ^[b]	k_{-1} [s^{-1}]	k_2 ^[c] [$\text{M}^{-1}\text{ s}^{-1}$] ^[e,f]	K [M^{-1}]
adc ^[d]	MeCN	870 855	(7.8 ± 0.2)		(3.4 ± 0.2) $\times 10^{-3}\text{ M}^{-1}\text{ s}^{-1}$	
btd ^[d]	MeCN	880	(8.1 ± 0.1) $\times 10^{-3}$		(1.9 ± 0.4) $\times 10^{-4}\text{ M}^{-1}\text{ s}^{-1}$	
dmad	MeCN	870	(35 ± 1)		(3.4 ± 0.4) $\times 10^{-3}\text{ M}^{-1}\text{ s}^{-1}$	38 ± 5
dmad	CH_2Cl_2	845 875	(8.0 ± 0.2)		(5.6 ± 0.5) $\times 10^{-4}\text{ M}^{-1}\text{ s}^{-1}$ ^[g]	
PrA	MeCN	898	(3.74 ± 0.07) $\times 10^{-3}$	(9 ± 1) $\times 10^{-5}$	(2.0 ± 0.1) $\times 10^{-4}\text{ s}^{-1}$	
PhA	MeCN	890	(3.3 ± 0.1) $\times 10^{-3}$	(2.7 ± 0.2) $\times 10^{-4}$	(1.1 ± 0.1) $\times 10^{-3}\text{ M}^{-1}\text{ s}^{-1}$	1.2 ± 0.4
PhA	CH_2Cl_2	890	(4 ± 1) $\times 10^{-3}$	(1.3 ± 0.4) $\times 10^{-3}$	(1.15 ± 0.04) $\times 10^{-3}\text{ M}^{-1}\text{ s}^{-1}$	
$^{\text{F}}\text{PhA}$	MeCN	892	(8.7 ± 0.2) $\times 10^{-3}$		— ^[h]	
$^{\text{CF}_3}\text{PhA}$	MeCN	892	(1.36 ± 0.07) $\times 10^{-2}$		(1.42 ± 0.04) $\times 10^{-4}\text{ s}^{-1}$	

[a] Maximum of the absorption band for the type I adduct. In cases where two wavelengths appear, they correspond to the position of the band for two different intermediates formed sequentially. The first wavelength corresponds to the first intermediate. [b] Appearance of the near-infrared absorption band. [c] Disappearance of the near-infrared absorption band. Depending on the alkyne, the rate constants for this step show saturation behavior with respect to the alkyne [the values of K in Eq. (2) are included in the table], or they are either zero or first order with respect to the alkyne, as indicated in the table by the corresponding units (i.e., $[\text{s}^{-1}]$ or $[\text{M}^{-1}\text{ s}^{-1}]$, respectively). [d] Data from reference [7]. [e] Three kinetic steps, the second one showing a shift of the band from $\lambda = 870$ to 855 nm . The rate constants for the second step show a dependence on the alkyne concentration of the type $a+b[\text{adc}]$ with $a = (4.7 \pm 0.6) \times 10^{-3}\text{ s}^{-1}$ and $b = (0.19 \pm 0.02)\text{ M}^{-1}\text{ s}^{-1}$. [f] In this case the value in the table actually corresponds to the third kinetic step. For adc the dependence is of the type $a+b[\text{adc}]$ with $a = (2.4 \pm 0.2) \times 10^{-4}\text{ s}^{-1}$ and the b value given in the table. [g] Three kinetic steps, the second one showing a shift of the band from $\lambda = 845$ to 875 nm . The rate constants for the second step are independent of the alkyne concentration, $k_{2\text{obs}} = (6 \pm 2) \times 10^{-3}\text{ s}^{-1}$. [h] The kinetic data for this step are not well-behaved.

analysis of the kinetic data for the second step had to be limited to the $\lambda = 700\text{--}1000$ nm wavelength range in order to isolate the reaction of interest from other independent spectral changes taking place at lower wavelengths that correspond to side reactions of reagents and byproducts (see the Supporting Information). Although the variety of rate laws observed for the second kinetic step can be always considered to result from simplification of Equation (2), the existence of interfering processes hinders a detailed analysis and no more efforts were dedicated to this point, the interest being focused on the first resolved kinetic step.

$$k_{1\text{obs}} = k_1[\text{alkyne}] \quad (1)$$

$$k_{2\text{obs}} = \frac{k_1[\text{alkyne}]}{1 + K[\text{alkyne}]} \quad (2)$$

$$k_{1\text{obs}} = k_1[\text{alkyne}] + k_{-1} \quad (3)$$

In order to study the effect of the solvent on the kinetics, the reaction was also monitored in dichloromethane solutions. The corresponding kinetic data are also included in Table 2 and the Supporting Information. No large differences with respect to acetonitrile were observed, except that an additional kinetic step is observed in the reaction with dmad. In such case, the spectral changes had to be fitted to three consecutive steps and the spectra calculated for the different species are included in Figure S9 in the Supporting Information. The major difference with respect to the other data in Table 2 is the existence of an intermediate kinetic step signaled by a shift in the band from $\lambda = 845$ to 875 nm and with a zero order with respect to the alkyne. The existence of three steps was previously observed for the reaction with adc in acetonitrile, and it was interpreted in terms of formation of a different type I adduct, probably by substitution of pyridine by a coordinated alkyne.^[7] In any case, the reaction of cluster $[1]^+$ with alkynes always leads initially to compounds showing an intense band in the near-infrared region. Shibahara and co-workers have reported that this band is typical of type I adducts,^[5] and recent time-dependent (TD) DFT calculations indicated that it can be assigned to charge-transfer transitions from the alkyne to the cluster core.^[6] Thus, the first step in the reaction of cluster $[1]^+$ with alkynes corresponds in all cases to a [3+2] cycloaddition process, a result that is further supported by the characterization of its type I adduct with dmad in CH_2Cl_2 by means of ^1H and $^{13}\text{C}\{^1\text{H}\}$ NMR and 2D HSQC and HMBC experiments (see the Supporting Information).

The data in Table 2 show that the rates of cycloaddition span over four orders of magnitude, the reaction being faster with the activated acetylenedicarboxylates typically used in click chemistry.^[12] The solvent appears to play a minor role, as changes are of less than an order of magnitude. For phenylacetylene and its derivatives, the rate increases with the number of electron-withdrawing substituents on the phenyl group but again it is a small increase, the rates for ^tPhA and $^{\text{CF}_3}\text{PhA}$ being only larger than for the unsubstituted alkyne by a factor of two or three, respectively. The rates of the cycloaddition

with btd and PrA only differ by a factor of two, thus showing that the rate of the reaction is not very different for related internal and terminal alkynes. It is also interesting to note that for some of the alkynes the kinetics of the cycloaddition reaction with cluster $[1]^+$ shows a non-zero intercept [Eq. (3)], and careful inspection of the spectral changes indicates that the magnitude of the changes increases with the concentration of the alkyne, thus showing that these reactions occur under conditions of reversibility. Actually, the values of the equilibrium constant for the cycloaddition process in acetonitrile solution derived from the k_1/k_{-1} quotient (41 and 12 M^{-1} for PrA and PhA, respectively) agree well with those obtained by fitting the total absorbance changes in the first kinetic step at the wavelength of the maximum to Equation (4) (24 and 15 M^{-1} for PrA and PhA, respectively).^[13]

$$\Delta\text{Abs} = \frac{[1^+]K\Delta\varepsilon[\text{alkyne}]}{1 + K[\text{alkyne}]} \quad (4)$$

in which $\Delta\varepsilon$ is the increase of the molar absorptivity occurring upon product formation.

DFT studies on the concerted [3+2] cycloaddition reactions between $[\text{M}_3\text{S}_4(\text{acac})_3(\text{py})_3]^+$ [$\text{M} = \text{Mo}$ ($[1]^+$), W ($[2]^+$)] clusters and alkynes

The same computational protocol previously^[7] used to study the concerted [3+2] cycloaddition reaction of cluster $[1]^+$ with adc and btd has been applied here to the reactions of compounds $[1]^+$ and $[2]^+$ with all the alkynes included in Table 1, and special attention has been paid to understand the reasons behind the markedly different behavior of both clusters.

The DFT study began with the optimization of the structures of the transition states and type I products of the reactions between $[\text{M}_3\text{S}_4(\text{acac})_3(\text{py})_3]^+$ [$\text{M} = \text{Mo}$ ($[1]^+$), W ($[2]^+$)] and the alkynes in Table 1. Those corresponding to the reaction between cluster $[1]^+$ and the alkynes dmad and PhA are shown in Figure 4, whereas Table 3 includes a summary of the computed activation (ΔG^\ddagger) and reaction (ΔG_r) free energies. Despite the wide variety of the alkynes used, the estimated differences in the ΔG^\ddagger and ΔG_r values of these reactions are relatively small (less than 10 kcal mol^{-1}), but the differences agree well with the experimental observations. Both from a kinetic and thermodynamic point of view the alkynes can be divided in two groups, adc and its methylated derivative dmad, and the remaining alkynes. It is noteworthy that for the second group of alkynes the ΔG_r values correspond to slightly endergonic processes, in spite of the fact that all of these do take place experimentally. This discrepancy, already observed in previous reports,^[6,7] does not necessarily disagree with the formation of type I cycloaddition products, as it could be explained by taking into account that both the excess of alkyne used in the experiments and the existence of subsequent exergonic transformations will drive the reaction towards product formation. The observation in the present work that the reactions with some of these alkynes actually occur under conditions of rever-

sible equilibria adds further support to this conclusion. Regarding the computed activation barriers ΔG^\ddagger , the significantly lower values for the reactions with *adc* and *dmad* are in agreement with the experimental rate constants given in Table 2, and can be explained by using the frontier molecular orbital arguments previously employed when comparing the reactions of cluster $[1]^+$ with *adc* and *btd*.^[7] Electron-withdrawing substituents lead to alkynes with HOMO and LUMO orbitals relatively lower in energy, and this allows for a stronger interaction with the cluster. Conversely, the data given in Table 2 also show that the symmetric or asymmetric nature of the alkyne does not correlate with the rate of the cycloaddition. Note that, for instance, the reactions with *btd* and *PhA* take place with similar activation barriers despite featuring different R and R' groups.

Table 4 includes a summary of the computed bond lengths directly involved in the cycle formation between cluster $[1]^+$ and the alkynes, both at the transition-state and the reaction product geometries. Interestingly, the values show again that despite the wide variety of alkynes used, no large differences are observed when the nature of the alkyne is changed. As expected, the major differences appear between internal and terminal alkynes, the latter leading to more unsymmetrical structures. Actually, previous results for the reaction with *adc* and *btd*,^[7] also confirmed now for *dmad*, show that for these symmetrical internal alkynes the cycloadditions take place through transition-state structures with $d(C1-S1) \approx d(C2-S2)$ and $d(Mo1-S1) \approx d(Mo1-S2)$ (see Scheme 1 for nomenclature), indicative of highly synchronous processes. The extent of synchronicity^[14] can be measured by computing, at the transition-state geometries, the differences in the C–S and Mo–S bond lengths

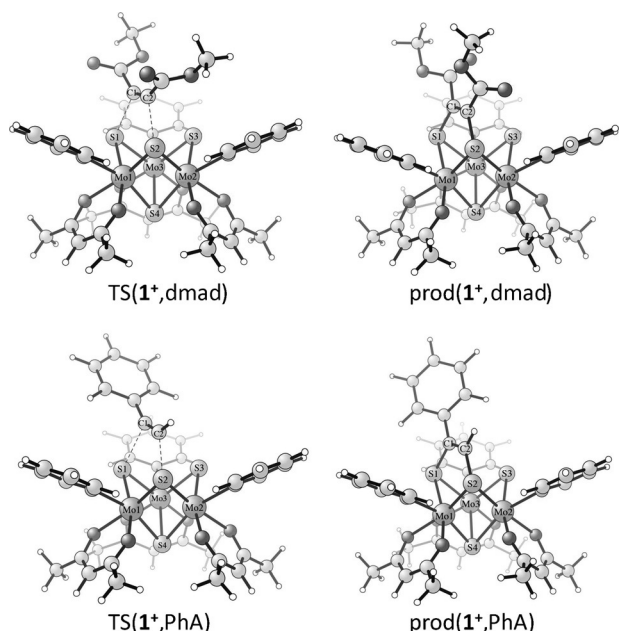


Figure 4. DFT-optimized structures of the transition states and type I products of the [3+2] cycloaddition reaction between cluster $[1]^+$ and the alkynes *dmad* and *PhA*. See the Supporting Information for a color version of this Figure.

Table 3. Activation (ΔG^\ddagger) and reaction (ΔG_r) free energies for the formation of type I reaction products between the clusters $[1]^+$ and $[2]^+$ with all the studied alkynes. The differences in these parameters, $\Delta\Delta G = \Delta G([2]^+) - \Delta G([1]^+)$, are also included. Values are given in [kcal mol⁻¹].

Alkyne	$[1]^+$		$[2]^+$		Difference	
	ΔG^\ddagger	ΔG_r	ΔG^\ddagger	ΔG_r	$\Delta\Delta G^\ddagger$	$\Delta\Delta G_r$
<i>adc</i>	13.3 ^[a]	-0.7 ^[a]	13.8	7.9	0.5	8.6
<i>dmad</i>	11.9	-2.1	14.3	8.4	2.5	10.5
<i>btd</i> ^[b]	21.9 ^[a]	6.0 ^[a]	24.3	16.5	2.4	10.5
<i>PrA</i>	23.1	5.3	27.1	15.7	4.0	10.4
<i>PhA</i>	21.6	4.9	24.8	16.3	3.2	11.4
<i>FPhA</i>	21.3	5.3	25.4	14.9	4.1	9.6
<i>CF₃PhA</i>	18.3	3.4	21.7	12.3	3.4	8.9

[a] Data from reference [7]. [b] For the reaction between cluster $[1]^+$ and *btd*, $\Delta E^\ddagger = 25.0$ and $\Delta E_r = 9.6$ kcal mol⁻¹. For the reaction between cluster $[2]^+$ and *btd*, $\Delta E^\ddagger = 30.6$ and $\Delta E_r = 21.4$ kcal mol⁻¹.

directly involved in the cycle formation [Eqs. (5) and (6)]. Values for the resulting parameters $\Delta r(C-S)$ and $\Delta r(Mo-S)$ are also included in Table 4, and they indicate that whereas the reactions with symmetric alkynes are essentially synchronous, cycloadditions with terminal alkynes are asynchronous processes with $\Delta r(C-S)$ values that reach up to 0.4 Å.^[15]

The highest degrees of asymmetry are clearly observed when one of the substituents of the alkyne is a phenyl group, the reaction with *PhA* (see TS($[1]^+$, *PhA*) in Figure 4) showing C...S distances as different as 2.169 and 2.573 Å ($\Delta r(C-S) = 0.404$ Å). Similar values are computed for the fluorinated derivatives of *PhA*, indicating that such functionalizations do not cause major structural or electronic changes. Conversely, the use of 2-propyn-1-ol (*PrA*), formally resulting from the substitution of one -CH₂OH moiety by -H in *btd*, only leads to a small increase in the $\Delta r(C-S)$ and $\Delta r(Mo-S)$ values, and this is probably due to the similar electron-donating properties of the -H and -CH₂OH moieties in relation to the cycle formation. In all cases, when moving from the transition states to the corresponding type I products, the differences in the C–S and Mo–S bond lengths are dramatically reduced, as shown by their small $\Delta r(C-S)$ and $\Delta r(Mo-S)$ values, which are also included in Table 4.

$$\Delta r(C-S) = |d(C1-S1) - d(C2-S2)| \quad (5)$$

$$\Delta r(Mo-S) = |d(Mo1-S1) - d(Mo1-S2)| \quad (6)$$

Nevertheless, the most striking result in the previously described experiments is the lack of reaction between the tungsten cluster $[2]^+$ and the alkynes under conditions similar to those employed for the molybdenum analogue $[1]^+$. Thus, DFT calculations have been carried out to understand the critical effect of the metal center in the [3+2] cycloaddition reaction, which is especially interesting because this is the only one of the five atoms participating in the [3+2] cycloaddition that does not participate directly in the bond formation with the alkyne. Firstly, the structures of the transition states and reaction products of the [3+2] cycloadditions between cluster $[2]^+$ and the alkynes given in Table 1 were computed. As an

Table 4. Summary of selected distances (*d*) and Δr values [Å] for the transition states and type I products of the [3+2] cycloaddition reaction between cluster [1]⁺ and the alkynes given in Table 1.^[a]

Distance	Internal alkynes			Terminal alkynes			
	adc ^[b]	dmad	btd ^[b]	PrA	PhA	^F PhA	^{CF₃} PhA
<i>d</i> (C1–C2)	1.211	1.211	1.211	1.208	1.211	1.211	1.210
	TS([1] ⁺ ,adc) ^[b]	TS([1] ⁺ ,dmad)	TS([1] ⁺ ,btd) ^[b]	TS([1] ⁺ ,PrA)	TS([1] ⁺ ,PhA)	TS([1] ⁺ , ^F PhA)	TS([1] ⁺ , ^{CF₃} PhA)
<i>d</i> (C1–C2)	1.256	1.256	1.254	1.253	1.26	1.261	1.259
<i>d</i> (C1–S1)	2.352	2.354	2.397	2.337	2.573	2.575	2.557
<i>d</i> (C2–S2)	2.393	2.394	2.386	2.407	2.169	2.168	2.169
<i>d</i> (Mo1–S1)	2.308	2.308	2.311	2.311	2.304	2.305	2.299
<i>d</i> (Mo1–S2)	2.305	2.306	2.307	2.308	2.326	2.327	2.328
Δr (C–S)	0.041	0.040	0.011	0.070	0.404	0.407	0.388
Δr (Mo–S)	0.003	0.002	0.004	0.003	0.022	0.022	0.029
	prod([1] ⁺ ,adc) ^[b]	prod([1] ⁺ ,dmad)	prod([1] ⁺ ,btd) ^[b]	prod([1] ⁺ ,PrA)	prod([1] ⁺ ,PhA)	prod([1] ⁺ , ^F PhA)	prod([1] ⁺ , ^{CF₃} PhA)
<i>d</i> (C1–C2)	1.338	1.337	1.336	1.332	1.337	1.337	1.335
<i>d</i> (C1–S1)	1.838	1.840	1.846	1.816	1.848	1.847	1.845
<i>d</i> (C2–S2)	1.846	1.841	1.842	1.835	1.811	1.812	1.811
<i>d</i> (Mo1–S1)	2.374	2.376	2.385	2.393	2.387	2.386	2.386
<i>d</i> (Mo1–S2)	2.381	2.385	2.380	2.393	2.391	2.393	2.393
Δr (C–S)	0.008	0.001	0.004	0.019	0.037	0.035	0.034
Δr (Mo–S)	0.007	0.009	0.005	0.000	0.004	0.007	0.007

[a] For cluster [1]⁺, *d*(Mo1–S1) = *d*(Mo2–S2) = 2.325 Å, as taken from reference [7]. [b] Data from reference [7].

example, graphical representations of the structures associated to the reaction with btd are shown in Figure 5, whereas Table S1 in the Supporting Information includes selected geometrical parameters for the remaining structures. A summary of all the computed activation and reaction free energies is given in Table 3, which also includes a comparison with the values for the same reactions of cluster [1]⁺.

As expected from the similar atomic and ionic radii of molybdenum and tungsten,^[16] a comparison of the structures computed for the [3+2] cycloadditions of clusters [1]⁺ and [2]⁺ shows in most cases bond length differences smaller than 0.1 Å.^[17] However, substitution of Mo by W has a clear effect on the energetics of the process. In agreement with the lack of reactivity with alkynes experimentally observed, the computed reaction free energies for cluster [2]⁺ are approximately 10 kcal mol⁻¹ higher than those for cluster [1]⁺, which now leads to clearly endergonic processes. Notably, the computed free energy barriers undergo a less pronounced increase of 0.5–4.1 kcal mol⁻¹, leading to values still typical of reactions observed at room temperature. All in all, the computations clearly indicate that the absence of a reaction between cluster [2]⁺

and the alkynes does not originate from high activation barriers (i.e., for kinetic reasons), but it has a thermodynamic origin.

Activation strain and energy decomposition analyses of the concerted [3+2] cycloaddition reaction between [M₃S₄(acac)₃(py)₃]⁺ (M = Mo ([1]⁺), W ([2]⁺)) clusters and btd

In order to gain greater insight into the origins of the difference in the reactivity of the clusters [1]⁺ and [2]⁺ with alkynes, their reactions with btd have been further analyzed by combining the activation strain model (ASM) analysis^[11] with the localized molecular orbital-energy decomposition analysis (LMO-EDA).^[18] The activation strain diagrams of both reactions, computed along the reaction coordinate *x* that connects the reactants and the products, are included in Figure 6.^[19] The two carbon–sulfur bond-forming distances leading to the type I cycloaddition product were selected as reaction coordinate *x* = *d*(C1–S1) = *d*(C2–S2) because they undergo a well-defined change throughout the reaction, being computed from 4.0 (close to non-interacting reactants) to 1.9 Å (near the cycloaddition products). Analysis of the electronic energy (ΔE) values

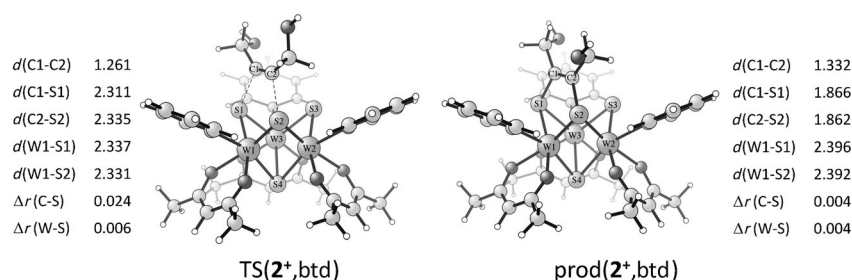


Figure 5. DFT-optimized structures of the transition-state (left) and type I product (right) geometries of the [3+2] cycloaddition reaction between cluster [2]⁺ and btd. Distances are given in [Å]. See the Supporting Information for a color version of this figure.

on the left-hand side of Figure 6a shows that the initial approach of the clusters (i.e., [1]⁺ or [2]⁺) and btd does not lead to stable adducts. Instead, a monotonic increase of similar magnitude is observed in both cases. This results from the addition of two unfavorable terms: the energy required to deform the reactants (Figure 6b), and the unfavorable interaction between them (Figure 6c). A gradual splitting of the two potential

energy surfaces (PESs) is, however, observed from reaction coordinate distances of approximately 2.9 Å (Figure 6a). As a result, at the section featuring the highest electronic energy values ($x \approx 2.3$ –2.4 Å) the ΔE_{max} values are about 5 kcal mol⁻¹ lower for the reaction of cluster [1]⁺ with btd than for cluster [2]⁺. At shorter distances both potential energy surfaces show a pronounced decrease in energy and continue to diverge, and in fact the difference in the relative energy reaches approximately 12 kcal mol⁻¹ at $x = 1.9$ Å.

Previous comparison^[7] of the activation strain diagrams for the reaction of cluster [1]⁺ with adc and btd has shown that during the course of these [3+2] cycloadditions (i.e., from $x = 4.0$ to 1.9 Å) there is a gradual increase in both the strain energy of the cluster [1]⁺ and the alkyne, with $\Delta E_{\text{strain}}([1]^+)$ being much smaller than $\Delta E_{\text{strain}}(\text{alkyne})$. This originates from the already-bent structure of the Mo(μ -S)₂ moiety, which does not have to deform in a large extent to reach product-like structures. Alkynes, on the other hand, have to undergo significant R–C≡C angle changes associated to the change in hybridization from sp to sp², largely contributing to the overall strain energy. A similar pattern is now observed for the reaction of cluster [2]⁺ with btd as shown in Figure 6b. In fact, the curves associated to $\Delta E_{\text{strain}}(\text{cluster})$ and $\Delta E_{\text{strain}}(\text{btd})$ in Figure 6b do not only coincide qualitatively, but the agreement is almost quantitative. This represents a somehow unexpected result with various implications: 1) the nature of the metal center in the cluster (i.e., clusters [1]⁺ or [2]⁺) does not have a significant effect on the energy required to deform the alkyne btd, 2) at least for the reaction with btd, the cost to deform both molybdenum and tungsten clusters is equal, 3) importantly, the similarity in the strain energies for the reaction of clusters [1]⁺ and [2]⁺ with btd as shown in Figure 6b means that the differences in the PESs of both reactions exclusively originate from those in the interaction energy, that is, the relative differences in the graphs in Figures 6a and c are approximately the same. Actually, Figure S20 in the Supporting Information shows a remarkable linear correlation between the differences in electronic [$\Delta E([2]^+, \text{btd}) - \Delta E([1]^+, \text{btd})$] and interaction [$\Delta E_{\text{int}}([2]^+, \text{btd}) - \Delta E_{\text{int}}([1]^+, \text{btd})$] energies of both reactions.

The localized molecular orbital energy decomposition analysis^[18] was employed at this point to further partition the interaction energies computed along the PESs into electrostatic (ΔE_{es}), exchange (ΔE_{ex}), repulsion (ΔE_{rep}), polarization (ΔE_{pol}), and dispersion (ΔE_{disp}) contributions (see the Experimental Section for details). Interestingly, such decomposition shows that the values of most of these contributions to the interaction energy for both reactions are almost identical along the PESs, and significant differences are in

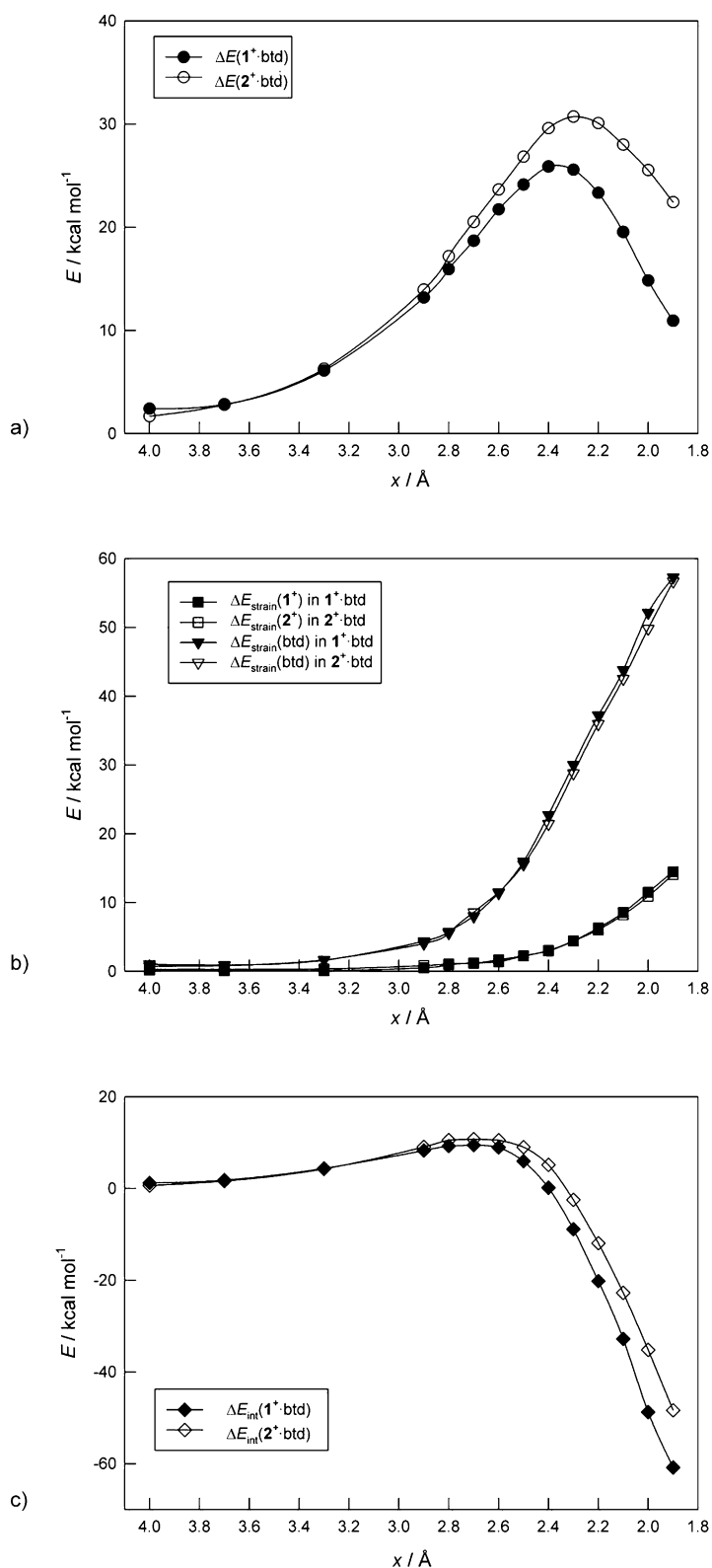


Figure 6. Activation strain diagrams for the reactions of clusters [1]⁺ (solid symbols) and [2]⁺ (open symbols) with btd. a) Total electronic energies, b) cluster and alkyne strain energies, and c) interaction energies along the reaction coordinate x [Å] projected onto the two forming C–S bonds. Note that different vertical scales were used. Energies are computed at the B3LYP/BS2(PCM)//B3LYP/BS1(PCM) level and given in [kcal mol⁻¹]. The data for the reaction between cluster [1]⁺ and btd were reproduced from reference [7].

fact only observed in the stabilizing ΔE_{pol} term (see individual plots in Figure S21 in the Supporting Information). This is graphically shown in Figure 7, where the differences in each of these contributions for the reaction of both clusters with btd have been plotted. Inspection of this figure reveals that the $\Delta\Delta E$ energies for the electrostatic, exchange, repulsion, and dispersion terms feature values near zero at all the computed C–S bond lengths, with the differences in the polarization energy ($\Delta\Delta E_{\text{pol}}$) starting to appear at the reaction coordinates of approximately 2.9 Å and accounting almost entirely for the difference in the interaction energy. The ΔE_{pol} term has its origin both in the empty–occupied orbital mixing within each fragment due to the presence of the other (polarization), and between the two fragments (charge transfer), thus indicating that the substitution of the Mo atoms in cluster [1]⁺ by tungsten in cluster [2]⁺ induces changes in the electronic structure of the cluster that result in weaker intra- and inter-fragment orbital interactions. Those changes become more pronounced as the two species get closer, leading to smaller energy differences at the transition-state geometries ($\approx 5 \text{ kcal mol}^{-1}$) than at the reaction products ($\approx 12 \text{ kcal mol}^{-1}$), and therefore affecting the thermodynamics more than the kinetics of the reaction.

The above-described conclusion is nicely supported from a frontier molecular orbital theory perspective. Inspection of the frontier orbitals of each fragment along the two PESs shows that their compositions do not change significantly with the metal center. In both cases the HOMO and LUMO of btd correspond to π and π^* orbitals mainly located at the $\text{C}\equiv\text{C}$

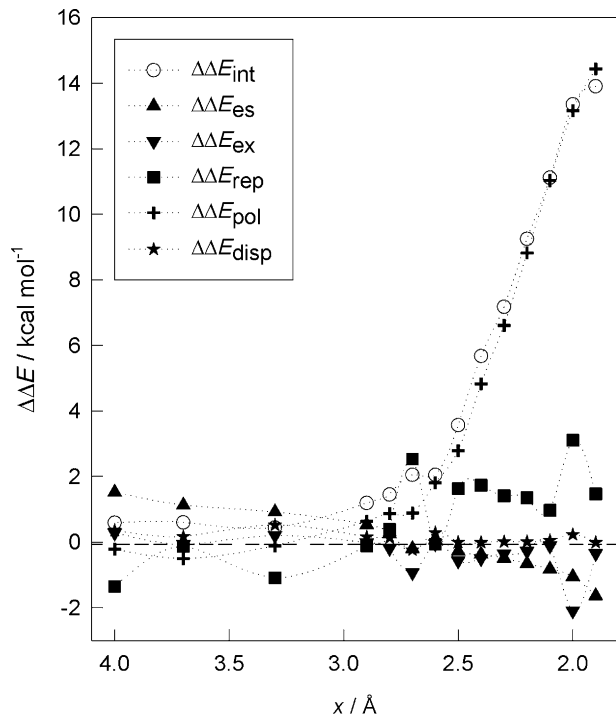


Figure 7. Plot of the differences in the interaction energy and their LMO-EDA-derived contributions, for the reactions of clusters [1]⁺ and [2]⁺ with btd along the reaction coordinate x [Å] projected onto the two forming C–S bonds. Energies are computed at the B3LYP/SBKJG/B3LYP/BS1(PCM) level and given in [kcal mol⁻¹].

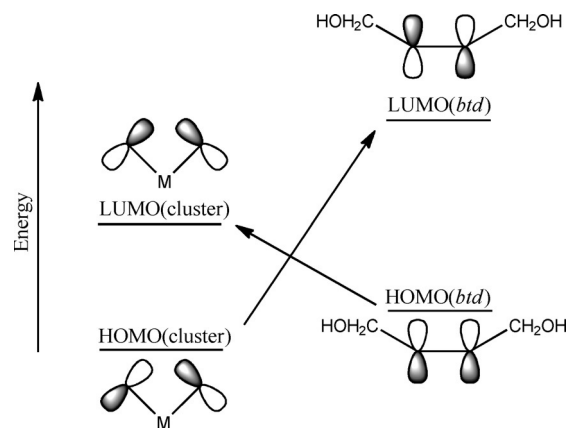


Figure 8. Schematic representation of the main orbital interactions in the reaction of the clusters [1]⁺ and [2]⁺ with btd. For clarity, only the MS_2 ($M = \text{Mo}, \text{W}$) moiety of the clusters has been represented. Full representations of these orbitals at the transition-state geometries are given in Figures S22 and S23 in the Supporting Information.

atoms. The HOMO and LUMO orbitals of both clusters are also similar, featuring most of the electron density at the $\text{M}(\mu\text{-S})_2$ moiety of the clusters that interact with the alkyne, being also partially delocalized among the other metal and $\mu\text{-S}$ atoms. As a result, regardless of the employed cluster there are two symmetry-allowed interactions favoring product formation (Figure 8), that is, a main $\text{HOMO}(\text{btd}) \rightarrow \text{LUMO}(\text{cluster})$ interaction that features the smaller gap and represents the major source of inter-fragment orbital stabilization, and a secondary $\text{HOMO}(\text{cluster}) \rightarrow \text{LUMO}(\text{btd})$ interaction with a larger gap and therefore lower impact on the interaction energies.

Thus, although this general picture holds for the reaction with both clusters, critical differences are observed in the energies of their frontier orbitals along the PESs, especially those of the cluster fragments. Note that, in agreement with the similar deformation energy associated with the alkyne btd in both reactions, its HOMO and LUMO energies are also equal along the PESs (Figure 9). Notably, the plots in Figure 9 clearly show how the gradual decrease in the $\text{R}-\text{C}\equiv\text{C}$ bond angles of the alkyne along the PESs mainly affects the energy of its LUMO, which becomes closer in energy to the HOMO of the clusters. Conversely, the HOMO and LUMO energies of the tungsten cluster [2]⁺ are systematically higher than those of the molybdenum cluster [1]⁺ by approximately 0.25 and 0.45 eV, respectively. This highlights the higher intrinsic stability of the molybdenum cluster [1]⁺ with respect to cluster [2]⁺, which translates within the LMO-EDA framework into a more effective empty–occupied orbital mixing within the cluster fragment. In addition, this also affects the empty–occupied orbital mixing between fragments and especially the main interaction (i.e., that with the smaller energy gap) between the $\text{HOMO}(\text{btd})$ and $\text{LUMO}(\text{cluster})$. Substitution of the molybdenum atoms in cluster [1]⁺ by tungsten in cluster [2]⁺ increases the LUMO energy of the cluster, leading to a less stabilizing interaction energy in the framework of the FMO theory, which is in agreement with the LMO-EDA results.

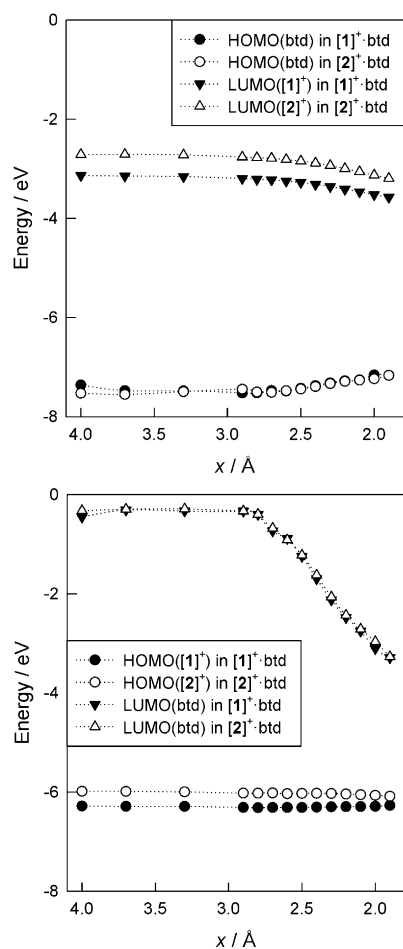


Figure 9. Evolution of the Kohn–Sham B3LYP/BS2//B3LYP/BS1(PCM) frontier orbital energies [eV] of the cluster $[1]^+$ or $[2]^+$ and btd along the reaction coordinate x [Å] projected onto the two forming C–S bonds. For clarity, the orbitals corresponding to each of the two HOMO–LUMO interactions between the clusters and btd have been plotted in different graphs.

Conclusion

The reactivity of the $[M_3S_4(acac)_3(py)_3]^+$ [$M = Mo$ ($[1]^+$), W ($[2]^+$)] clusters with alkynes is drastically affected by the nature of the metal, the Mo cluster reacting with all tested alkynes and the W analogue being unreactive with all of them. The reactions of cluster $[1]^+$ show polyphasic kinetics, but in all cases the first step corresponds to the formation of species bearing a bridging dithiolene through the concerted [3+2] cycloaddition between the sp-hybridized carbon atoms of the alkyne and a $Mo(\mu-S)_2$ moiety of the cluster. The rate of this cycloaddition is highly dependent on the employed alkyne, and the relative values for the different alkynes are well explained by DFT calculations on the basis of the different electron-withdrawing properties of the substituents, which drastically affect the extent of orbital interaction between the two species at the transition-state geometry. In agreement with the experimental results, the computations also show that, although the symmetrical or unsymmetrical nature of the alkyne has an effect on the synchronicity of the processes, no clear correlation with the computed activation barriers exists.

The computations on the reactions of the tungsten cluster $[2]^+$ with the alkynes feature activation barriers only slightly higher (between 0.5 and 4.1 kcal mol⁻¹) than the ones of cluster $[1]^+$, whereas the differences in the reaction free energies increase up to approximately 10 kcal mol⁻¹. This clearly indicates that the different reactivity observed for the Mo and W clusters has a thermodynamic origin. Surprisingly, the results of the ASM analysis show negligible differences in the strain energies of the clusters [$\Delta E_{\text{strain}}(\text{cluster})$] and the alkyne [$\Delta E_{\text{strain}}(\text{btd})$] when the nature of the transition metal is changed, the difference in the reactivity being in fact solely explained on the basis of their interaction energies ΔE_{int} . These start to diverge when the two reactants approach to each other and continue to do so up to the reaction products, leading to smaller energy differences at the transition-state geometries than at the reaction products. The LMO-EDA analysis shows that the differences in the interaction energies between the Mo and W clusters are only due to the ΔE_{pol} term, so that it can be concluded that the changes in the electronic structure of the cluster caused by substitution of the Mo atoms by W lead to weaker intra- and inter-fragment orbital interactions. All in all, the results of the present work show that cycloaddition reactions of these clusters with alkynes are on the borderline of being thermodynamically favored or not, which opens the possibility of tuning the reactivity by changing the nature of the ancillary ligands or the solvent.

Experimental Section

General remarks

The clusters $[Mo_3S_4(acac)_3(py)_3]PF_6$ ($[1]PF_6$) and $[W_3S_4(acac)_3(py)_3]PF_6$ ($[2]PF_6$) were prepared following the literature procedure.^[20] Dimethyl acetylenedicarboxylate, propargyl alcohol, phenylacetylene, 1-ethynyl-4-fluorobenzene, and 1-ethynyl-3,5-bis(trifluoromethyl)benzene were purchased from Aldrich and used as received without further purification.

NMR studies

NMR spectra were recorded on Agilent 500 and 600 DD2 equipment. Chemical shifts are given in parts per million from $SiMe_4$ (1H and $^{13}C\{^1H\}$) or $CFCl_3$ (^{19}F). 1H and $^{13}C\{^1H\}$ NMR signal assignments were confirmed by 1H -gCOSY, g-HSQC, and g-HMBC experiments. Reactions were carried out under an Ar atmosphere following standard Schlenk techniques, although the resulting compounds are not particularly sensitive to air or humidity.

Kinetic experiments

The kinetic experiments were carried out with an Applied Photo-physics SX-17MV stopped-flow spectrometer provided with a PDA1 photodiode array detector, and with a Cary 50 Bio UV/Vis spectrophotometer. All experiments were carried out at $(25.0 \pm 0.1)^\circ C$ in acetonitrile and dichloromethane by mixing a solution of the cluster $[(0.6\text{--}3.0) \times 10^{-4} M]$ with another solution containing the alkyne in a concentration range large enough $[(0.01\text{--}0.40) M]$ to ensure pseudo-first order conditions. Preliminary experiments at two different cluster concentrations were carried out to confirm the first-order dependence of the observed rate constants on this reagent.

The spectral changes in the range $\lambda = 700\text{--}1000$ nm were analyzed with the software Specfit,^[21] satisfactory fits usually requiring of kinetic models with more than one consecutive kinetic steps, as indicated for each reaction in the Results and Discussion section.

DFT calculations

The DFT calculations were performed by using Gaussian 09.^[22] Geometry optimizations were carried out at the B3LYP/BS1 level of theory^[23] without any symmetry constraint, and included the effects of the solvent (CH₃CN, $\epsilon = 35.688$) self-consistently through the polarizable continuum model (PCM).^[24] The basis set system BS1 employs the SDD relativistic ECP and associated basis set for Mo, W, and S atoms,^[25] with added polarization functions for the latter ($\zeta = 0.503$),^[26] and the 6-31G** basis set for C, O, and hydrogen atoms.^[27] All stationary points were characterized through analytical frequency calculations as either minima (all positive eigenvalues) or transition states (one negative eigenvalue), and intrinsic reaction coordinate (IRC) calculations and subsequent geometry optimizations were used to confirm the minima linked by each transition state. In order to obtain improved energetic values all energies were recomputed through single-point calculations with a larger basis set system, BS2, also including solvent effects (PCM).^[24] BS2 differs from BS1 in the employment of the 6-311+G(2d,2p) level for the C, O, and hydrogen atoms. Solution free energies were obtained by adding zero-point and thermal effects at 298.15 K (at the B3LYP/BS1(PCM) level of theory), as well as D3(BJ) dispersion effects,^[28] to the electronic energies resulting from the B3LYP/BS2(PCM) single-point calculations.

The activation strain model (ASM)^[11] was employed to gain more insights into the different contributions to the PESs associated with the formation of different type I reaction products. ASM analyses were performed in terms of electronic energies relative to the separated reactants (ΔE), and can be applied to stationary and non-stationary structures. Note that when applied to the latter, these are typically computed along a reaction coordinate x that connects reactants and products. In either case, the method consists of dissecting the energy of each selected structure into strain (ΔE_{strain}) and interaction energy (ΔE_{int}) [Eq. (7)]:

$$\Delta E = \Delta E_{\text{strain}} + \Delta E_{\text{int}} \quad (7)$$

The strain energy represents the energy penalty for adopting a distorted geometry by the reactants, and can therefore be dissected in the present case into $\Delta E_{\text{int}}(\text{cluster})$ and $\Delta E_{\text{int}}(\text{alkyne})$ [Eq. (8)]:

$$\Delta E_{\text{strain}} = \Delta E_{\text{strain}}(\text{alkyne}) + \Delta E_{\text{strain}}(\text{cluster}) \quad (8)$$

whereas the interaction energy accounts for the energy associated to the covalent and noncovalent interactions between those species. In this work all the activation strain results were obtained by using the same methodology as indicated before, that is, optimizations were carried out at the B3LYP/BS1(PCM) level, followed by B3LYP/BS2(PCM) single-point energy calculations.

The localized molecular orbital energy decomposition analysis, developed by Su and Li,^[18] has been used to partition the previously computed interaction energies of the PESs for the reactions between the clusters [1]⁺ and [2]⁺ with btd into electrostatic (ΔE_{es}), exchange (ΔE_{ex}), repulsion (ΔE_{rep}), polarization (ΔE_{pol}), and dispersion (ΔE_{disp}) components [Eq. (9)]:

$$\Delta E_{\text{int}} = \Delta E_{\text{es}} + \Delta E_{\text{ex}} + \Delta E_{\text{rep}} + \Delta E_{\text{pol}} + \Delta E_{\text{disp}} \quad (9)$$

The electrostatic energy represents the interaction between the static charge densities (i.e., nucleus–nucleus and electron–electron repulsion as well as nucleus–electron attraction) of each fragment within the supermolecule, and it is usually stabilizing (attractive). The exchange component refers to the quantum mechanical exchange between electrons of the same spin, and it is counteracted by the repulsion energy, which originates from the fact that two electrons with the same spin cannot occupy the same region in space. These two terms, which are stabilizing and destabilizing, respectively, are gathered together in the original Kitaura–Morokuma method^[29] and many other EDA methods.^[30] The polarization term corresponds to the stabilizing effect caused by relaxation of the fragment orbitals upon binding, and includes empty–occupied orbital mixing within one fragment due to the presence of another (polarization) and between two fragments (charge transfer). The dispersion term as computed in the LMO-EDA method is a stabilizing term that arises from electron correlation, and in combination with DFT methods it is defined by using the changes in the employed correlation functional on going from the separated fragments to the supermolecule.^[18]

LMO-EDA calculations on the previously B3LYP/BS1(PCM) geometries were performed by using the GAMESS program package.^[31] These calculations employed the B3LYP exchange–correlation functional^[23] and the Stevens–Basch–Krauss–Jasien–Cundari effective core potentials and corresponding valence double- ζ basis sets.^[32] The Boys and Bernardi counterpoise method,^[33] as implemented in the LMO-EDA method, was employed to correct for the basis set superposition error (BSSE). Note that the ΔE_{int} values thus computed differ slightly from those obtained at the B3LYP/BS2(PCM)//B3LYP/BS1(PCM) level of theory (from Gaussian 09 calculations) due to the differences in the treatment of the solvation effects and superposition error, as well as the different basis set systems.

Acknowledgements

Financial support by the Junta de Andalucía (Group FQM-137), the Spanish MICINN, and European Union FEDER program (project CTQ2012-37821-C02) is gratefully acknowledged. The University of Cádiz is acknowledged for computing time.

Keywords: cluster compounds · cycloaddition · density functional calculations · kinetics · reaction mechanisms

- [1] a) P. Metzner, A. Thuillier, in *Sulfur Reagents in Organic Synthesis*, Academic Press, San Diego, **1994**, pp. 195–200; b) K. Matsumoto, H. Sugiyama, *Acc. Chem. Res.* **2002**, *35*, 915–926; c) K. Matsumoto, H. Sugiyama, *J. Organomet. Chem.* **2004**, *689*, 4564–4575; d) M. Arisawa, K. Fujimoto, S. Morinaka, M. Yamaguchi, *J. Am. Chem. Soc.* **2005**, *127*, 12226–12227; e) A. Correa, O. Garcia Mancheno, C. Bolm, *Chem. Soc. Rev.* **2008**, *37*, 1108–1117; f) Y. Jiang, T.-P. Loh, *Chem. Sci.* **2014**, *5*, 4939–4943; g) C. Shen, P. Zhang, Q. Sun, S. Bai, T. S. A. Hor, X. Liu, *Chem. Soc. Rev.* **2015**, *44*, 291–314; h) L. Wang, W. He, Z. Yu, *Chem. Soc. Rev.* **2013**, *42*, 599–621.
- [2] a) A. Stanislaus, A. Marafi, M. S. Rana, *Catal. Today* **2010**, *153*, 1–68; b) C. Song, *Catal. Today* **2003**, *86*, 211–263; c) K. G. Knudsen, B. H. Cooper, H. Topsoe, *Appl. Catal. A* **1999**, *189*, 205–215.
- [3] a) S.-Y. Yan, Y.-J. Liu, B. Liu, Y.-H. Liu, Z.-Z. Zhang, B.-F. Shi, *Chem. Commun.* **2015**, *51*, 7341–7344; b) I. P. Beletskaya, V. P. Ananikov, *Chem. Rev.* **2011**, *111*, 1596–1636; c) F. Pan, H. Wang, P.-X. Shen, J. Zhao, Z.-J. Shi, *Chem. Sci.* **2013**, *4*, 1573–1577; d) M. Wang, C. Fu, S. Ma, *Chem. Sci.* **2013**, *4*, 1016–1022.
- [4] a) C. Shen, H. Xia, H. Yan, X. Chen, S. Ranjit, X. Xie, D. Tan, R. Lee, Y. Yang, B. Xing, K.-W. Huang, P. Zhang, X. Liu, *Chem. Sci.* **2012**, *3*, 2388–

- 2393; b) L. Yang, Q. Wen, F. Xiao, G.-J. Deng, *Org. Biomol. Chem.* **2014**, *12*, 9519–9523; c) C. Shen, J. Xu, W. Yu, P. Zhang, *Green Chem.* **2014**, *16*, 3007–3012; d) Z. Weng, W. He, C. Chen, R. Lee, D. Tan, Z. Lai, D. Kong, Y. Yuan, K.-W. Huang, *Angew. Chem. Int. Ed.* **2013**, *52*, 1548–1552; *Angew. Chem.* **2013**, *125*, 1588–1592.
- [5] a) T. Shibahara, H. Akashi, A. Toupadakis, D. Coucouvanis, in *Inorganic Syntheses*, Wiley, New York, **1992**, pp. 260–269; b) T. Shibahara, G. Sakane, S. Mochida, *J. Am. Chem. Soc.* **1993**, *115*, 10408–10409; c) M. Maeyama, G. Sakane, R. Pierattelli, I. Bertini, T. Shibahara, *Inorg. Chem.* **2001**, *40*, 2111–2119; d) Y. Ide, M. Sasaki, M. Maeyama, T. Shibahara, *Inorg. Chem.* **2004**, *43*, 602–612; e) H. Takagi, Y. Ide, T. Shibahara, *Comptes Rendus Chimie* **2005**, *8*, 985–992; f) Y. Ide, T. Shibahara, *Inorg. Chem.* **2007**, *46*, 357–359; g) T. Shibahara, K. Kawamoto, A. Matsuura, H. Takagi, T. Nishioka, I. Kinoshita, H. Akashi, *Bull. Chem. Soc. Jpn.* **2014**, *87*, 459–469.
- [6] J. Á. Pino-Chamorro, A. G. Algarra, M. J. Fernández-Trujillo, R. Hernández-Molina, M. G. Basallote, *Inorg. Chem.* **2013**, *52*, 14334–14342.
- [7] J. Á. Pino-Chamorro, A. L. Gushchin, M. J. Fernández-Trujillo, R. Hernández-Molina, C. Vicent, A. G. Algarra, M. G. Basallote, *Chem. Eur. J.* **2015**, *21*, 2835–2844.
- [8] a) J. McMaster, J. M. Tunney, C. D. Garner, in *Dithiolene Chemistry*, Wiley, New York, **2004**, pp. 539–583; b) J. M. Tunney, J. McMaster, C. D. Garner, in *Comprehensive Coordination Chemistry II, Vol. 8* **2004**, Elsevier, Amsterdam, pp. 459–477.
- [9] a) R. Llusar, V. Polo, E. Velez, C. Vicent, *Inorg. Chem.* **2010**, *49*, 8045–8055; b) R. Llusar, S. Triguero, V. Polo, C. Vicent, C. J. Gómez-García, O. Jeannin, M. Fourmigué, *Inorg. Chem.* **2008**, *47*, 9400–9409; c) A. Alberola, R. Llusar, S. Triguero, C. Vicent, M. N. Sokolov, C. Gómez-García, *J. Mater. Chem.* **2007**, *17*, 3440–3450; d) R. Llusar, S. Triguero, C. Vicent, M. N. Sokolov, B. Domerq, M. Fourmigué, *Inorg. Chem.* **2005**, *44*, 8937–8946; e) R. Llusar, S. Uriel, C. Vicent, J. M. Clemente-Juan, E. Coronado, C. J. Gómez-García, B. Braïda, E. Canadell, *J. Am. Chem. Soc.* **2004**, *126*, 12076–12083; f) S. Bruña, I. Cuadrado, E. Delgado, C. J. Gómez-García, D. Hernández, E. Hernández, R. Llusar, A. Martín, N. Menéndez, V. Polo, F. Zamora, *Dalton Trans.* **2014**, *43*, 13187–13195; g) D. Recatalá, A. L. Gushchin, R. Llusar, F. Galindo, K. A. Brylev, M. R. Ryzhikov, N. Kitamura, *Dalton Trans.* **2013**, *42*, 12947–12955.
- [10] a) D. H. Ess, *J. Org. Chem.* **2009**, *74*, 1498–1508; b) M. A. Celik, R. Haunschild, G. Frenking, *Organometallics* **2010**, *29*, 1560–1568; c) R. Haunschild, G. Frenking, *J. Organomet. Chem.* **2009**, *694*, 4090–4093; d) R. Haunschild, G. Frenking, *J. Organomet. Chem.* **2008**, *693*, 3627–3637; e) R. Haunschild, S. Tüllmann, G. Frenking, M. C. Holthausen, *J. Organomet. Chem.* **2009**, *694*, 1081–1090; f) R. Haunschild, G. Frenking, *J. Organomet. Chem.* **2008**, *693*, 737–749; g) R. Haunschild, C. Loschen, S. Tüllmann, D. Cappel, M. Hölscher, M. C. Holthausen, G. Frenking, *J. Phys. Org. Chem.* **2007**, *20*, 11–18; h) D. Cappel, S. Tüllmann, C. Loschen, M. C. Holthausen, G. Frenking, *J. Organomet. Chem.* **2006**, *691*, 4467–4473; i) M. Hölscher, W. Leitner, M. C. Holthausen, G. Frenking, *Chem. Eur. J.* **2005**, *11*, 4700–4708.
- [11] a) F. M. Bickelhaupt, E. J. Baerends, N. M. M. Nibbering, T. Ziegler, *J. Am. Chem. Soc.* **1993**, *115*, 9160–9173; b) F. M. Bickelhaupt, *J. Comput. Chem.* **1999**, *20*, 114–128; c) I. Fernández, F. M. Bickelhaupt, *Chem. Soc. Rev.* **2014**, *43*, 4953–4967; d) L. P. Wolters, F. M. Bickelhaupt, *WIREs Comput. Mol. Sci.* **2015**, *5*, 324–343.
- [12] a) R. L. Melen, D. W. Stephan, *Dalton Trans.* **2015**, *44*, 5045–5048; b) V. Nair, R. S. Menon, P. B. Beneesh, V. Sreekumar, S. Bindu, *Org. Lett.* **2004**, *6*, 767–769; c) R. Berger, M. Wagner, X. Feng, K. Mullen, *Chem. Sci.* **2015**, *6*, 436–441; d) L. Henry, C. Schneider, B. Mutzel, P. V. Simpson, C. Nagel, K. Fucke, U. Schatzschneider, *Chem. Commun.* **2014**, *50*, 15692–15695; e) S. A. Knott, J. N. Templeton, J. L. Durham, A. M. Howard, R. McDonald, L. F. Szczepura, *Dalton Trans.* **2013**, *42*, 8132–8139.
- [13] K. A. Connors, *Binding Constants, the Measurement of Molecular Complex Stability*, Wiley, New York, **1987**.
- [14] a) W. T. Borden, R. J. Loncharich, K. N. Houk, *Annu. Rev. Phys. Chem.* **1988**, *39*, 213–236; b) M. J. S. Dewar, *J. Am. Chem. Soc.* **1984**, *106*, 209–219.
- [15] Despite the asynchronicity of these cycloadditions, IRC analyses assert their one-step nature.
- [16] G. Raj, *Advanced Inorganic Chemistry, Vol. 1*, Krishna Prakashan Media, Meerut, **2014**.
- [17] The major difference in the bond lengths appear on the transition states computed for the reactions of cluster [2]⁺ with adc and dmad. This is due to the different orientation of the –COOR (R=H, Me) groups of the alkynes in the optimized structures, which in the present case, induce a large degree of asynchronicity (see the Supporting Information).
- [18] P. Su, H. Li, *J. Chem. Phys.* **2009**, *131*, 014102.
- [19] These approaches do not make use of free but electronic energies (see values in Table 3). There is, however, a clear parallelism between these magnitudes, ensuring that the analyses are indeed very useful to rationalize the differences in reactivity.
- [20] R. Hernández-Molina, M. Sokolov, W. Clegg, P. Esparza, A. Mederos, *Inorg. Chim. Acta* **2002**, *331*, 52–58.
- [21] SPECFIT-32, R. A. Binstead, B. Jung, A. D. Zuberbühler, Spectrum Software Associates, Chappel Hill, **2000**.
- [22] Gaussian 09, Revision A.02, M. J. Frisch, G. W. Trucks, H. B. Schlegel, G. E. Scuseria, M. A. Robb, J. R. Cheeseman, G. Scalmani, V. Barone, B. Mennucci, G. A. Petersson, H. Nakatsuji, M. Caricato, X. Li, H. P. Hratchian, A. F. Izmaylov, J. Bloino, G. Zheng, J. L. Sonnenberg, M. Hada, M. Ehara, K. Toyota, R. Fukuda, J. Hasegawa, M. Ishida, T. Nakajima, Y. Honda, O. Kitao, H. Nakai, T. Vreven, J. A. Montgomery, Jr., J. E. Peralta, F. Ogliaro, M. Bearpark, J. J. Heyd, E. Brothers, K. N. Kudin, V. N. Staroverov, R. Kobayashi, J. Normand, K. Raghavachari, A. Rendell, J. C. Burant, S. S. Iyengar, J. Tomasi, M. Cossi, N. Rega, J. M. Millam, M. Klene, J. E. Knox, J. B. Cross, V. Bakken, C. Adamo, J. Jaramillo, R. Gomperts, R. E. Stratmann, O. Yazyev, A. J. Austin, R. Cammi, C. Pomelli, J. W. Ochterski, R. L. Martin, K. Morokuma, V. G. Zakrzewski, G. A. Voth, P. Salvador, J. J. Dannenberg, S. Dapprich, A. D. Daniels, O. Farkas, J. B. Foresman, J. V. Ortiz, J. Cio-slawski, D. J. Fox, Gaussian Inc., Wallingford CT, **2009**.
- [23] a) A. D. Becke, *J. Chem. Phys.* **1993**, *98*, 5648–5652; b) C. T. Lee, W. T. Yang, R. G. Parr, *Phys. Rev. B* **1988**, *37*, 785–789.
- [24] a) J. Tomasi, B. Mennucci, R. Cammi, *Chem. Rev.* **2005**, *105*, 2999–3093; b) M. Cossi, G. Scalmani, N. Rega, V. Barone, *J. Chem. Phys.* **2002**, *117*, 43–54.
- [25] D. Andrae, U. Haussermann, M. Dolg, H. Stoll, H. Preuss, *Theor. Chim. Acta* **1990**, *77*, 123–141.
- [26] A. Höllwarth, M. Bohme, S. Dapprich, A. W. Ehlers, A. Gobbi, V. Jonas, K. F. Kohler, R. Stegmann, A. Veldkamp, G. Frenking, *Chem. Phys. Lett.* **1993**, *208*, 237–240.
- [27] a) P. C. Hariharan, J. A. Pople, *Theor. Chim. Acta* **1973**, *28*, 213–222; b) W. J. Hehre, R. Ditchfield, J. A. Pople, *J. Chem. Phys.* **1972**, *56*, 2257–2261.
- [28] a) S. Grimme, J. Antony, S. Ehrlich, H. Krieg, *J. Chem. Phys.* **2010**, *132*, 154104; b) S. Grimme, S. Ehrlich, L. Goerigk, *J. Comput. Chem.* **2011**, *32*, 1456–1465.
- [29] K. Kitaura, K. Morokuma, *Int. J. Quantum Chem.* **1976**, *10*, 325–340.
- [30] a) M. J. S. Phipps, T. Fox, C. S. Tautermann, C.-K. Skylaris, *Chem. Soc. Rev.* **2015**, *44*, 3177; b) H. Hirao, *Chem. Phys. Lett.* **2007**, *443*, 141–146; c) W. J. Stevens, W. H. Fink, *Chem. Phys. Lett.* **1987**, *139*, 15–22; d) R. Z. Khaliullin, E. A. Cobar, R. C. Lochan, A. T. Bell, M. Head-Gordon, *J. Phys. Chem. A* **2007**, *111*, 8753–8765; e) Y. Mo, J. Gao, S. D. Peyerimhoff, *J. Chem. Phys.* **2000**, *112*, 5530–5538.
- [31] M. W. Schmidt, K. K. Baldrige, J. A. Boatz, S. T. Elbert, M. S. Gordon, J. H. Jensen, S. Koseki, N. Matsunaga, K. A. Nguyen, S. Su, T. L. Windus, M. Dupuis, J. A. Montgomery, *J. Comput. Chem.* **1993**, *14*, 1347–1363.
- [32] a) W. J. Stevens, H. Basch, M. Krauss, *J. Chem. Phys.* **1984**, *81*, 6026–6033; b) T. R. Cundari, W. J. Stevens, *J. Chem. Phys.* **1993**, *98*, 5555–5565; c) W. J. Stevens, M. Krauss, H. Basch, P. G. Jasien, *Can. J. Chem.* **1992**, *70*, 612–630.
- [33] S. F. Boys, F. Bernardi, *Mol. Phys.* **1970**, *19*, 553–566.

Received: July 6, 2015

Published online on September 7, 2015